Characteristics of 16 Beetle1.1 chips on a VELO hybrid

23rd January 2004

S. Klous[a,b], N. van Bakel[a], D. Baumeister[c,†], M. van Beuzekom[a], H.J. Bulten[a,b], E. Jans[a], T.J. Ketel[a,b], S. Löchner[c], S. Mos[a], H. Snoek[a,b], U. Trunk[d], H. Verkooijen[a], H. de Vries[a], M. Zupan[a].

[a] NIKHEF, P.O. Box 41882, 1009 DB Amsterdam, The Netherlands
[b] Vrije Universiteit Amsterdam, The Netherlands
[c] Max-Planck-Institute for Nuclear Physics, Heidelberg, Germany
[d] Physics Institute University of Heidelberg, Germany

Abstract

This note presents the results of beam-test measurements performed with a prototype VELO hybrid equipped with 16 Beetle1.1 chips. A 300 μm thick PR02-R p-on-n detector is used as sensor. The front-end settings of the chip were tuned to meet the LHCb vertex detector requirements. The pulse shape that complies best with LHCb specifications has a signal/noise ratio of 17.9, a spill-over of 36.1% and a rise time of 23.5 ns. Channel-dependent effects were studied with data from high statistics measurements. High trigger rate and single time sample measurements were analyzed to investigate specific aspects under LHCb conditions.

Contents

† Present address: Continental Teves AG, Frankfurt, Germany

1 Introduction

The Beetle1.1 is a radiation hard read-out chip with an analog pipeline that is designed to operate at 40 MHz. It implements the RD-20 front-end architecture [1]. The Beetle has been designed for the LHCb vertex detector, but will also be used by the pile-up detector, the trigger tracker and the inner tracker of LHCb. Measurements were done with a hybrid containing 16 Beetle1.1 chips in the 120 GeV pion beam at the X7 facility at CERN [2] in August 2002. These measurements are part of a study investigating the compliance of the Beetle chip with the LHCb vertex detector requirements. The purposes of the experiment were to study the system response to minimum ionizing particles (MIPs) and to use 16 chips on a single hybrid.

The Beetle has several parameters that can be used to tune pulse shape characteristics like rise time, signal/noise ratio and spill-over. The most important parameters are the pre-amplifier current (I_{pre}), the shaper current (I_{sha}) and the feedback resistance of the shaper (controlled by V_{fs}) [3]. The pre-amplifier was operated at its maximum possible current of 350 μA, as explained in section 2. Based on results from previous experiments [4] a shaper current of 32 μA was selected to create a pulse shape with at maximum 15% undershoot. This is a compromise between the height of the pulse and the remainder after 25 and 50 ns. An overview of the data is presented in Table 1.

Table 1: All data sets as measured in the experiment. I_{sha} = 32 μA, I_{pre} = 350 μA.

	Type	V_{fs} [mV]	Events [M]
1	Pulse shape scan, chips 8, 9, 10, 13, 14, 15	500-800	1.4
2	High statistics runs, chips 8, 9, 10, 13, 14, 15	700	1.0
3	Pulse shape scan, all chips	500-800	1.6
4	Single time sample runs	700	1.0
5	High trigger rate runs	700	1.0
	Total		6.0

Data set 1 was used to tune the feedback resistance of the shaper (V_{fs}) and to find an optimized pulse shape for the vertex detector. Data set 2 was measured with high statistics and is used to investigate channel dependencies and determine systematic errors. Data set 3 is used to obtain results for all chips. Data sets 4 and 5 are the single time sample and high trigger rate measurements respectively, both are used to investigate specific aspects of LHCb operation and to cross-check the results.

This report has the following structure: Section 2 gives a description of the setup used in the beam-test. In section 3 noise studies are presented. Section 4 discusses the pulse shape parametrization and section 5 presents the pulse shape analysis including all cross-checks and results. Finally, in section 6 conclusions are drawn.

2 Experimental setup

A prototype VELO hybrid has been designed at NIKHEF and was constructed by Eltech [5] to test 16 Beetle1.1 chips in a beam environment. For the experiment the system was extended with two scintillators and an XY station with HELIX chips [6], as shown in Fig. 1. The Beetle off-detector electronics was close to the beam, the rest of the data acquisition system was about 8 meters away.

A 300 μm thick PR02-R p-on-n detector was used as sensor. It consists of 2048 strips divided in 16 sectors as shown in Fig. 2, each of which is read-out by one Beetle chip. The inner radius and outer radius of the detector are 8.0 mm and 42.2 mm, respectively. The strip width is about 40% of the pitch, which varies from 32.5 μm in the inner regions to 92 μm in the outer regions. The detector was biased at 150 V which is 110 V above the depletion voltage. We refer to this detector as “the Beetle detector”.

A two layer pitch adapter is used as a transition between the detector pitch (2 rows of bond pads, effective pitch = 61.5 μm) and the chip pitch (4 rows of bond pads, effective pitch = 40.24 μm). The pitch adapter consists of a 200 μm thick epoxy substrate on top of which a 50 μm thick kapton layer is glued. The pitch adapters were glued on 200 μm thick aluminum plates with the same shape to flatten them before they were mounted on the hybrid. By accident the aluminum plates are left electrically floating, which introduces additional noise (see section 3.1).

The chip design is based on a 0.25 μm CMOS integrated circuit technology. The 16 Beetle1.1 chips were bonded without prior testing. They are all fully operational, which indicates a high yield of this deep sub-micron technology. The clock frequency of the chips is 40 MHz, equal to the bunch crossing frequency of LHC. They are read-out in single port

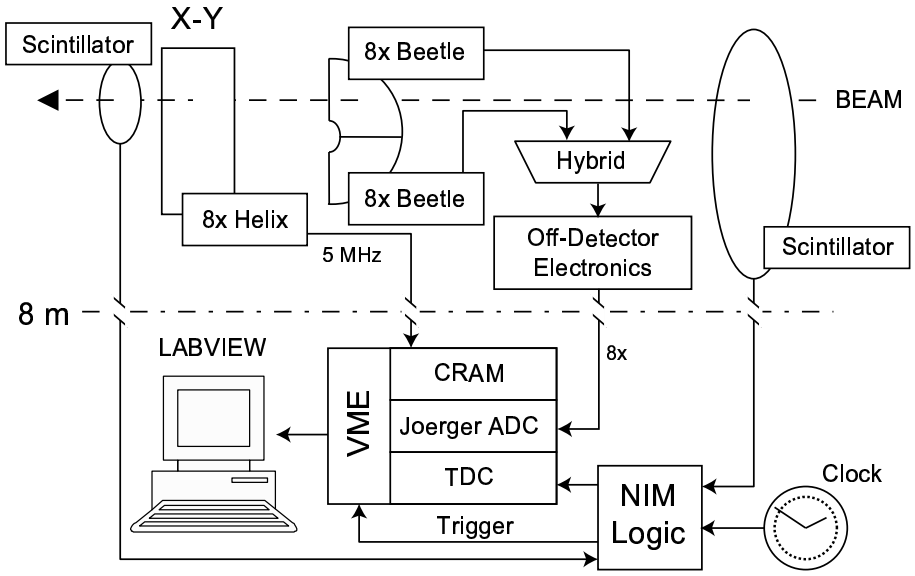

Figure 1: Overview of the setup used in the beam-test.

mode, which means the signals from 128 channels are serialized to reduce the number of ADC channels needed. Each read-out starts with an 8 bit header pattern. A functional diagram of the Beetle is shown in Fig. 3. It contains the front-end circuit of one channel, one of the pipeline cells and the read-out. A dummy channel is shown as well which is the same as the other channels, but without a pre-amplifier. It corrects for common-mode noise that originates in the chip.

The pulse shape characteristics and signal/noise ratio are mainly determined by the transfer function of the front-end circuit. The time-constants and gain of this circuit can be adjusted with the pre-amplifier current, the shaper current and the feedback resistance of the shaper. These settings are programmed with an I^2C interface [7] via 10 bits on-chip Digital to Analog Converters (DAC). The pre-amplifier is operated at its maximum possible current of 350 μA[1] . A detailed description of the Beetle chip can be found in [3].

The hybrid consists of a four-layer printed circuit board with kapton insulation layers of 75 μm thickness and a copper thickness of 17 μm. Connections between the hybrid and the off-detector electronics (ODE) board are made via flexible cables called tails, one of which was fabricated from solid copper and the other one from copper with a grid. On the ODE board, about 30 cm from the Beetle chips, the line-drivers amplify the signals by a factor 36. A group of 8 signals can be amplified simultaneously; jumpers are used for selection.

The silicon sensors need to be operated in a light-tight enclosure. Cooling is enforced by circulating air in the box with a ventilator to obtain an operational temperature of about 35°C. The signals are sent over 8 meter long cables to the 8 channel, 12 bit ADC VME-module (Joerger VTR812-40). Two broken ADC-inputs reduced the total available number of ADC channels to 6.

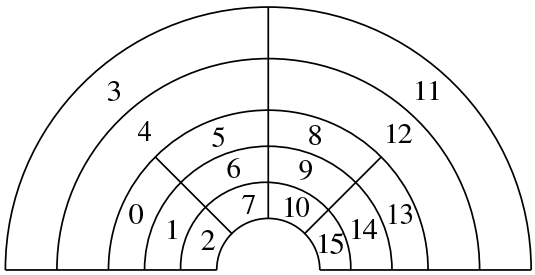

Figure 2: Layout and sector numbering of the Beetle detector.

[1]This pre-amplifier current limit is due to saturation of the DAC circuitry in the Beetle1.1. The corresponding DAC settings are: DAC_{pre} = 600 (for a pre-amplifier current of 350 μA) and DAC_{sha} = 50 (for a shaper current of 32 μA). The Beetle1.2 shows no saturation up to the maximum design value of 2 mA for the current [10].

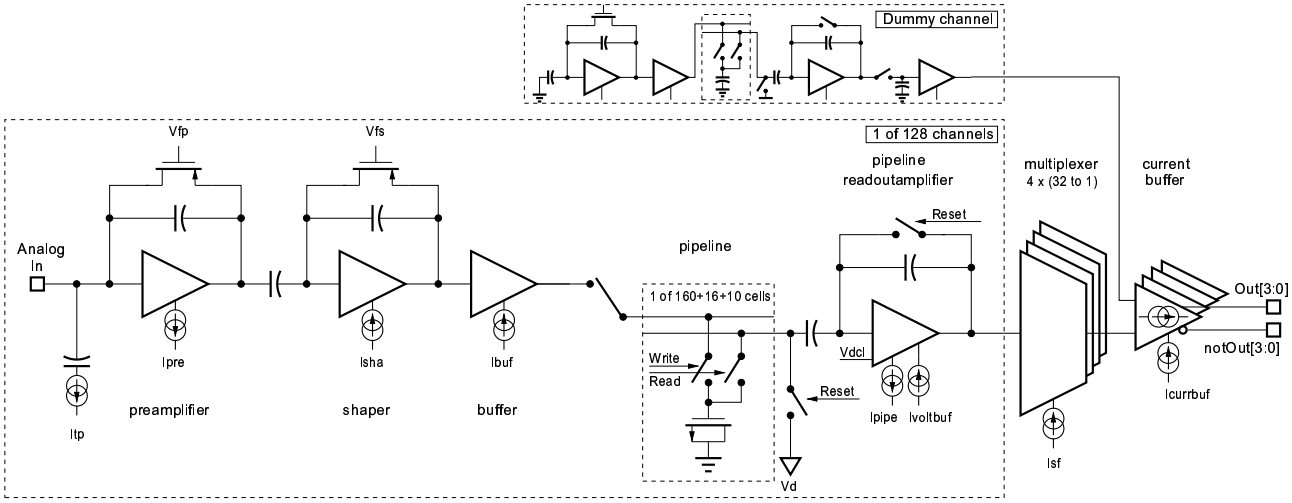

Figure 3: Functional diagram of the Beetle1.1.

An XY tracking station with a surface area of 6×12 cm^2 provides an additional space-point for each track. This tracking station consists of two detector planes mounted back to back with a strip pitch of 20 μm and a read-out pitch of 120 μm. Read-out is done by HELIX chips connected to a CAEN V550 10 bit VME-ADC (CRAM) operating at 5 MHz.

Triggers are constructed from a coincidence between the signals from two scintillators. A TDC measures the time difference between the trigger and the rising edge of the next Beetle clock pulse. Since the beam is continuous in the spill, the TDC information can be used to reconstruct the transient response of the Beetle chip. For the majority of the data, a single trigger issued the read-out of 8 consecutive time samples of 25 ns, spanning a total period of 200 ns. In this way the complete pulse shape is reconstructed from the data, without the need to change the latency. A data acquisition program written in LABVIEW, controls a non-graphical C-based program capable of collecting up to 500 events per spill of 5 seconds.

3 Noise studies

In order to obtain a correct interpretation of the data it is important to understand the noise characteristics of the system. Measurements of the noise give a first indication about the quality and uniformity of the setup and the chip response. Noise originates in the detector, the Beetle chip, the line-drivers and in the Joerger ADC module that is used in the data acquisition. In addition noise can be picked up by the hybrid and the pitch-adapter and by the cables that connect the Beetle to the Joerger ADC. In the plots of this chapter, measurements with Beetle settings I_{sha} = 32 μA, I_{pre} = 350 μA and V_{fs} = 700 mV are shown.

3.1 Total noise

The distribution of the pedestal-subtracted signal of a time sample is presented in Fig. 4. This time sample precedes the samples that contain the pulse. The noise is highly symmetric and Gaussian distributed with a normalized χ^2 of ≈ 1.09. The distributions are qualitatively the same for all Beetle chips at all settings. The standard deviation of the Gaussian is called “total noise”, which is determined for each channel and each time sample separately.

For every trigger, the ADC takes 24 samples before the data from the Beetle arrive. These samples can be used to determine the so-called “system noise", *i.e.* noise generated in the Joerger ADC or by the line-drivers. This noise depends on the Joerger input used, and varies from file to file. Typically it is around 6 ADC counts, with the exception of Joerger input 7 which has been used to read-out chip 7 or 15, where the noise varies between 7 and 14 ADC counts due to ground loop currents. No attempt was made to subtract this noise.

Fig. 5 shows the standard deviation of the distribution of the pedestal-subtracted signal as a function of channel number for chip 1. The distributions of the other chips look similar. Some features are apparent:

- The first 4 channels of the chip have a high total noise. Histograms with the pedestal-subtracted signals of these channels show two peaks, which are caused by a pedestal shift that is correlated with the sign of the last header bit.

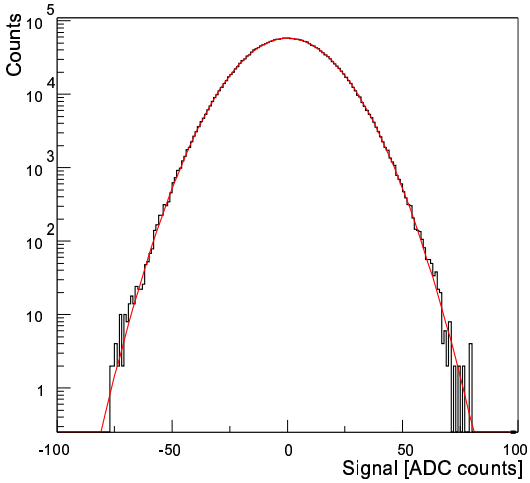

Figure 4: Pedestal-subtracted signals for 10k events in Beetle chip 0. The distribution is fitted with a Gaussian.

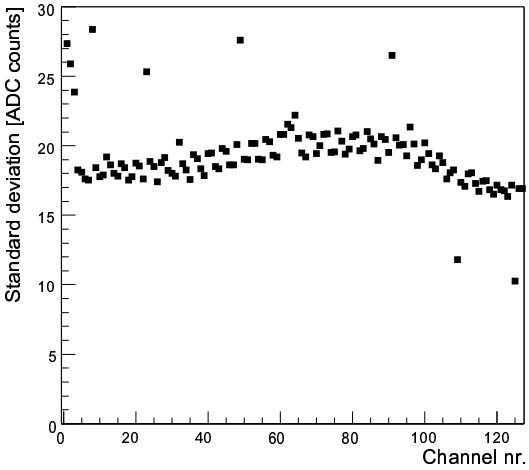

Figure 5: Total noise for 10k events in chip 1 versus channel number.

More detailed studies show that the signal of the first channel contains an oscillation that fades out when the sample time is delayed. This ringing of the external amplifiers is presumably caused by insufficient phase margin or gain bandwidth [8]. The external amplifiers used, are operated at their limit because of the very small output signal of the Beetle1.1. An independent measurement showed that reflections on the analogue read-out cables disturb the signal of the first four channels. A tuned system (impedance, amplifiers and signal termination) in combination with the four times larger amplification factor of future chip versions will eliminate this problem. From here on data of the channels 0, 1, 2, and 3 are rejected in the analysis of all chips.

- Some chips have channels with a noise around 12 ADC counts and/or with much higher noise than the average. The channels with low noise correspond to unbonded channels, the channels with high noise probably suffer from cross-talk with the neighboring routing line or bond. In section 3.2 more detailed information about these anomalous channels can be found.
- The total noise as a function of channel number has a double band structure. In a group of 4 consecutive channels, the first two channels have on average about 10% more noise than the last two. This structure matches the layout of the pitch adapter, where the first two channels of each group of 4 are routed over the lower layer and the last two over the upper layer. The higher noise in the lower layer is due to the floating aluminum plate on which the pitch adapter was glued. This issue was further investigated in two steps. First, a similar double band structure was formed with an RF generating setup in an independent measurement. A high frequency oscillator generated a 5 MHz RF signal at the open end of a coaxial-line positioned at the center of the detector. Second, two bonds were swapped on the chip side of the pitch adapter and two bonds of other channels on the silicon side. In the former case the additional noise moved to a different channel while in the latter nothing changed. This indicates that the RF pick-up as well as the noise leading to this double band structure originate in the pitch adapter.
- The noise of chips connected to sensor regions with long strips (chip 3, 4, 11 and 12) is up to 10% higher than the noise of chips connected to the shorter strips in the inner region, which have less input capacitance [9].

In order to compare the absolute noise values for different chips, a gain factor was determined based on the difference in ADC value between high and low header bits. This difference is independent of chip settings and was in our measurements about 80 times larger than the noise. The gain factors are typically between 0.85 and 1.15. From here on, the noise that is shown is gain-corrected.

3.2 Noise anomalies

The data of the channels listed in Table 2 were excluded from the analysis due to anomalous noise effects. Channel numbers 0 to 3 are excluded for all chips due to ringing in the external amplifiers and reflections on the analog output cables as discussed in section 3.1. Channel numbers 0, 32, 64 and 96 are excluded for all chips because they pick up a few percent extra noise due to a multiplexer feature (which is solved in the Beetle1.2) [10]. Channels with broken bonds

can easily be identified, because they have a noise around 12 ADC counts (34 channels). An RF generating setup was used to study the response of these channels. The test confirmed that these channels do not respond to the RF signal. This supports the conclusion that these channels suffer from bonding problems instead of problems with chip internals or read-out electronics. Other channels (41 in total) have extra noise due to shorts with the neighboring channels in either the bonds, the silicon sensor or the pitch adapter. It was verified that the noise of these channels returns to a nominal value when the bond of the neighboring channel is removed. On average we excluded 11.7 channels per chip (9.1%). Some of the chips have no additional anomalous channels, while others have as much as 16 extra channels with problems.

Table 2: Overview of all excluded channels.

Chip number	Excluded channels
All	0, 1, 2, 3, 32, 64, 96
0	56, 57
1	8, 23, 49, 62, 63, 91, 109, 125
2	12, 24, 56, 125
3	11, 20, 24, 25, 34, 36, 40, 48, 71, 72, 101
4	4, 8, 41, 42, 43, 57, 68, 108, 109, 112
5	5, 120, 121
6	29, 74, 84
7	80
8	
9	17, 25, 73
10	84, 104, 106
11	5, 7, 9, 12, 16, 18, 19, 24, 28, 30, 57, 77, 81, 109, 112, 122
12	48, 49, 92, 125
13	25, 41, 72, 74, 88, 112
14	
15	92

3.3 Common-mode noise correction

Subtraction of common-mode noise is required to correct for low-frequency noise that is picked up by the read-out electronics or the silicon detector. Four different strategies were investigated. Common to all four is the elimination of channels that contain a hit. In this case a channel is said to contain a hit when its ADC value is larger than 5 times the total noise of that channel and time sample. The four different strategies are described below.

1. The average pedestal subtracted signal of the channels of one chip is subtracted from the data.
2. The pedestal subtracted signal is fitted with a first-order polynomial as a function of read-out channel number. This corrects for a common-mode picked up between the chip and the ADC that slowly varies in time ($\sim$ kHz), since the channels are read-out sequentially.
3. The pedestal subtracted signal is fitted with a first-order polynomial as a function of strip length. This corrects for a linear dependence of common-mode pickup on strip capacitance.
4. Individual weight factors are determined for each channel by constructing a spectrum with on the x-axis the common-mode corrected noise in a channel and on the y-axis the common-mode noise as calculated with method 1. A straight line is fitted to the average values to determine the correlation. The correction factor is one plus the slope of this line. If this slope equals zero, the channel is weighted by a factor 1 and it picks up just the average amount. If the slope equals -1, the channel picks up no common-mode noise at all.

The common-mode noise for a chip is Gaussian distributed, with a σ of around 10 ADC counts. Correction of the data for common-mode noise reduces the noise per channel with about 13%. This effect differs slightly from file to file and from chip to chip. The extra reductions that can be obtained by applying the strategies 2, 3, and 4 amount to about 1%, 0.6%, and 2%, respectively. This is to be expected from the fact that a second fit parameter was introduced, hence the

Table 3: Results of the noise studies using 40k events. The standard deviation of the pedestal subtracted ADC-spectrum is given for different common-mode strategies. The column labeled "System noise" contains the average system noise as described in the text. The column "No correction" represents the results when no common-mode subtraction is applied. All values are in ADC counts.

Chip nr.	System noise	No correction	Strategy			
			1	2	3	4
0	5.1	19.3	16.6	16.4	16.5	16.3
1	6.1	20.7	17.7	17.5	17.6	17.3
2	5.5	19.0	16.3	16.2	16.2	16.0
3	6.1	22.0	19.5	19.3	19.2	19.1
4	6.9	21.3	18.7	18.6	18.6	18.3
5	6.0	20.1	16.9	16.7	16.8	16.5
6	6.8	21.3	17.0	16.8	16.9	16.6
7	8.1	19.3	16.7	16.5	16.6	16.4
8	5.5	21.3	16.8	16.6	16.7	16.5
9	7.2	19.4	16.8	16.6	16.7	16.5
10	4.7	21.3	16.0	15.9	15.9	15.8
11	5.8	22.7	20.0	19.8	19.8	19.5
12	5.9	20.8	18.7	18.6	18.6	18.4
13	5.5	18.4	16.1	15.9	16.0	15.8
14	5.3	17.9	15.8	15.7	15.7	15.5
15	10.6	17.7	15.9	15.8	15.8	15.7

improvement should be in the order of $N_{d.o.f.}^{-1} \approx 1\%$ (where $N_{d.o.f.}$ represents the number of degrees of freedom). Table 3 summarizes the results, obtained by analyzing 40k events.

As mentioned before, the straight-forward common-mode subtraction performed in strategy 1 yields a close to optimal result; more involved strategies like strategy 4 give negligible improvement. However, for historical reasons strategy 2 is applied: instead of a constant factor, a straight line is fitted through the pedestal-subtracted ADC data as function of the chip channel number.

In the rest of this section the channel to channel variations in the noise of the chips are discussed in detail. Figure 6 shows the total noise and the noise corrected for common-mode with strategy 2. A clear channel dependence is visible. As in the pedestal-subtracted signal, the first two channels in a group of 4 are noisier than the last two. Of course fitting a constant or straight line common-mode term does not remove this feature but blurs it a bit. Furthermore, after common-mode correction the noise of channels with channel numbers above 120 increases. These features are observed in all settings studied. During an independent measurement the Beetle was programmed to send only the data of the first 32 channels over the output line. The observed pattern matched exactly with that of the first 32 channels as presented in Fig. 6. This excludes the possibility that the higher noise in the channel numbers above 120 is the result of tail effects in the off-detector or DAQ electronics. Lab-measurements will be done for future chip versions, to investigate whether this problem can be attributed to the inhomogeneity of the noise in the pipeline cells [11].

The data from the channels that seem unconnected or pick up anomalous extra noise are rejected. Weight correlation factors are calculated for all the remaining channels. These weight factors are shown in Fig. 7. Here, the apparent structure shows up again: the first two channels in a group of 4 pick up more common-mode noise than the last two channels. The channels at the end of the chip pick up hardly any common-mode at all. When these corrections are applied in the common-mode subtraction, the noise of the channels with channel numbers above 120 is still higher than the noise of the rest of the channels. Although the weight factors typically deviate quite a lot from 1, the result yields on average only 1% extra reduction of the noise. This is due to the fact that the common-mode noise has an RMS of about 10 ADC counts; a 20% difference in the weight factor modifies the common-mode noise only by about 2 ADC counts. This correction is uncorrelated with the other noise sources, which contribute about 16 ADC counts to the noise. As mentioned, the common-mode algorithm using the weighted pickup is quite complex and the improvements are minimal, hence this method is not used in the rest of the analysis.

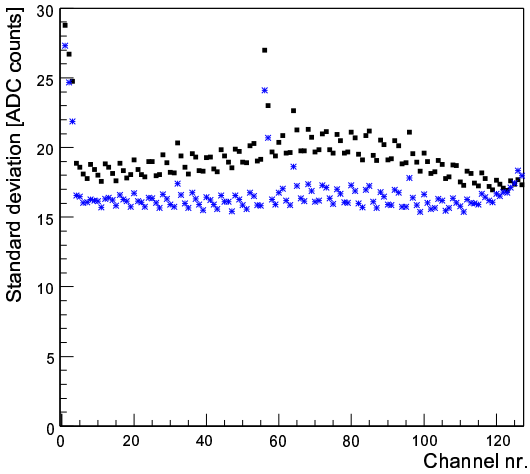

Figure 6: The total noise (black squares) and the common-mode subtracted noise (blue stars) in chip 0 as a function of channel number.

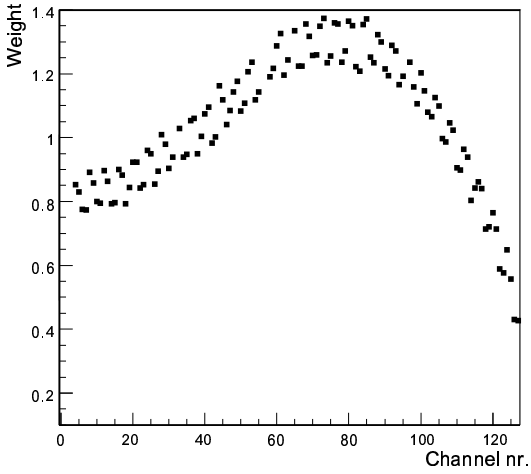

Figure 7: The weight factors as a function of channel number for the channel-dependent common-mode subtraction in strategy 4.

4 Pulse shape parametrization

The charge deposition of a particle that traversed the detector is identified with three different methods which are described in section 5. The collected charge is expressed in units of signal/noise ratio to allow for easy comparison between the performance of various settings and chips. The signal/noise ratios are stored in a two dimensional histogram of amplitude versus time as shown in Fig. 8. A selected event gives 8 entries in this histogram each 25 ns apart. Figure 8 is divided in slices of 3 ns along the x-axis to reconstruct the transient response of the Beetle chip with sufficient time resolution.

From each slice, a 1 dimensional histogram is constructed with the number of entries versus amplitude. These so-called energy-loss distributions have a Landau shape convoluted with a Gaussian for the peak of the pulse. The baseline is Gaussian, with a width of about 1. Details of this distribution are discussed in section 4.1. The characterization of the pulse shape is discussed in section 4.2.

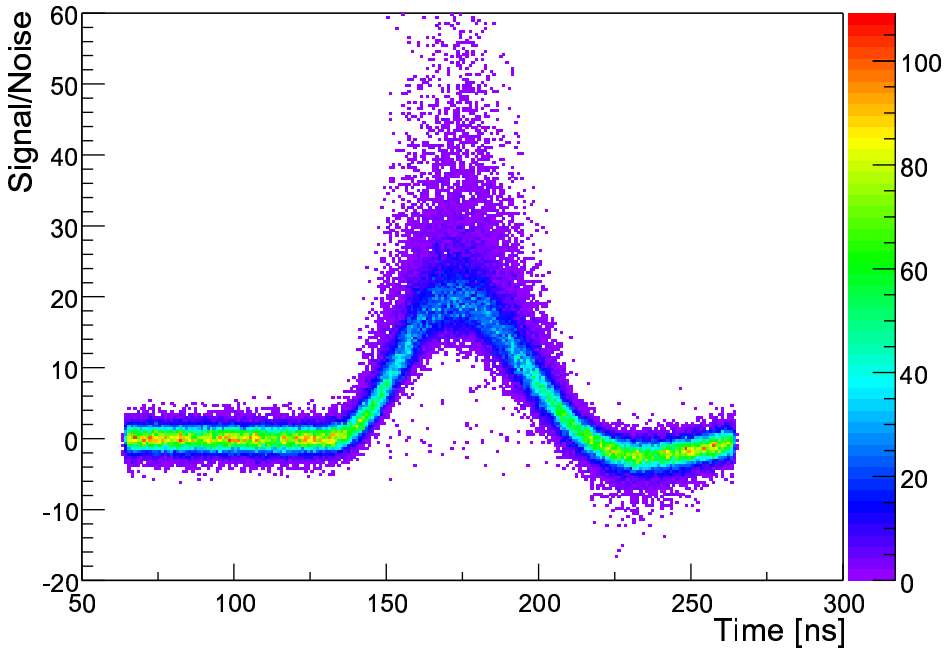

Figure 8: Two dimensional histogram of amplitude versus time.

4.1 Energy-loss distribution

The energy-loss distribution of a minimum ionizing particle passing through a thin slab of material is in first approximation described by the Landau probability density function [12]. Landau used a one-parameter model to describe the energy deposition of a traversing particle based on the properties and geometry of the stopping material. The binding energy of the electrons is neglected. As a consequence, the width of the distribution is underestimated. A practical solution is to broaden the Landau by means of a convolution with a Gauss [13]. In addition this convolution will account for noise contributions. These need to be disentangled when the results are compared to future measurements.

The convolution has four fit parameters: the most probable value (MPV) of the Landau, the width of the Landau, the width of the Gauss and a normalization parameter. The width and MPV of the Landau are decoupled for convenience [14]. The MPV of the convolution, which is quoted as signal/noise value, is a non-trivial combination of the fit parameters. This value is higher than the MPV of the Landau, its statistical error needs to be calculated using the covariance matrix of the fit in combination with the sensitivity for the fit parameters [16]. In Fig. 9 a typical energy-loss distribution in the peak of the pulse is shown together with the fitted convolution of a Landau and a Gauss. The convolution is performed with a numerical integration that uses Gaussian quadrature, based on an optimal distribution of the abscissa. This method is superior to trapezoid or Newton-Cotes integration methods which are based on equally spaced abscissa [15], especially in the rising edge and tail of the pulse where the width of the Landau becomes small.

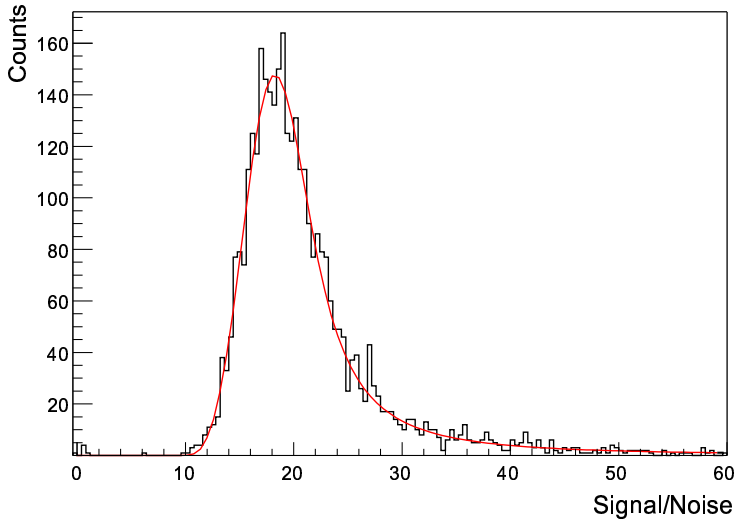

Figure 9: Typical energy-loss distribution in the peak of the pulse, fitted with the convolution of a Landau and Gauss.

4.2 Pulse shape characteristics

In Fig. 10 the MPV of each convolution is plotted versus the mean time of the slice it belongs to. From this kind of figures the pulse shape characteristics are extracted. The most interesting characteristics for LHCb are: rise time, signal/noise ratio and spill-over. Rise time is defined as the time difference between the moments where the pulse height amounts to 10% and 90% of the maximum pulse height. Signal/noise ratio is the maximum pulse height divided by the width of the noise in the baseline. Spill-over is the value of the pulse height 25 ns after the pulse reached its maximum height divided by the maximum pulse height. These parameters are extracted using a 6^{th} order polynomial fit to the data in Fig. 10. This function gives a reasonable description of the data. The curve is on average very close to the high precision data points. The normalized χ^2 of this fit is 3.3 because of a slight mismatch in the rising edge and the peak of the pulse. The small over-estimation in the peak value is about 0.1 in signal/noise ratio, which is included in the systematic error. The pulse shape characteristics are extracted numerically. The statistical errors of these characteristics are determined in first order with the covariance matrix of the polynomial fit and the sensitivity to the fit parameters [16]. The pulse is divided in slices of 3 ns as mentioned in section 4. The effects of varying the width of the slices and the bin locations are found to be: $\pm$ 0.1 for the signal/noise ratio, $\pm$ 1% in absolute value for the spill-over, $\pm$ 0.5 ns for the rise time. These results are also included in the systematic error.

In Fig. 10 a simulated pulse shape of the Beetle1.1 is shown as well. The simulation is normalized to the height of the measured pulse shape. The accuracy of the simulated time response is estimated to be about 10%. More details about this and other simulations can be found in section 5.1.

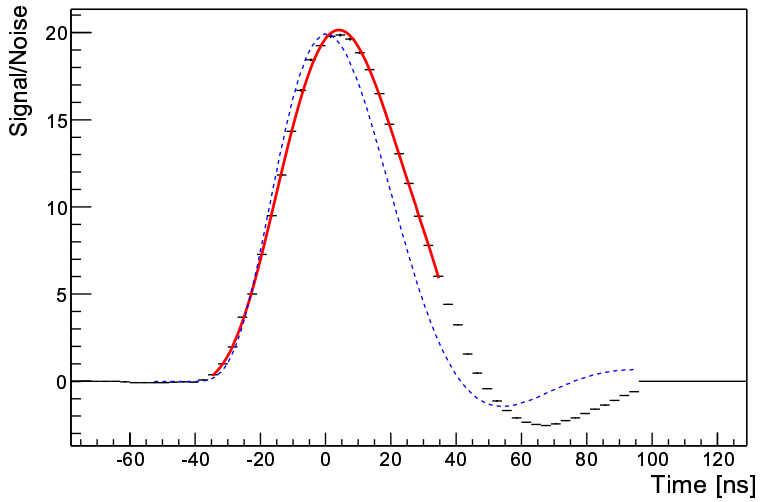

Figure 10: Most Probable Value (MPV) of the convolution plotted versus the mean time of the slice, together with the simulated pulse shape of the Beetle 1.1 (dashed line). The solid line is a 6^{th} order polynomial fit through the MPVs. I_{sha} = 32 µA, I_{pre} = 350 µA and V_{fs} = 700 mV.

5 Analysis

The analysis tools make extensive use of the classes provided by the VeloROOT software [17] of the LHCb VELO group. The tools are customized for things like data format and detector geometry to analyze the data produced by the Beetle chips and the XY station. The various histograms are created using a customized ROOT Tree [18] containing the events produced by the Beetles, extended with analysis methods to perform a.o. pedestal calculation, common-mode calculation and signal extraction. The preferred method to determine the Beetle pulse shape is via reconstruction of the cluster charges as a function of time. This method, which is explained in section 5.1, is used for the fast majority of the data, because it generates the 'cleanest' distributions. The problem with this method is the risk of overestimating the performance. Adding the signal/noise ratio of a neighboring strip, only when its value is above a certain threshold can introduce a bias toward higher signal/noise ratios [19]. The results from our cluster charge analysis are compared to a strip charge analysis in section 5.2 and to a track selection analysis in section 5.3 to identify possible systematic effects. Furthermore, measurements were done to test the compliance with single time sample and with high trigger rate conditions, as required for LHCb operation (see section 5.4 and 5.5). In section 5.6 a plot is presented and discussed that shows efficiency and spill-over as a function of threshold. This plot allows for a more direct estimate of the physics performance of the vertex detector if equipped with Beetle chips.

5.1 Cluster charge analysis

In the cluster charge analysis clusters are formed that represent the probability to find a hit at the reconstructed position. The signal/noise ratios of the selected strips are linearly added. This is mathematically equivalent to adding all the charge of a cluster and dividing it by the linear average of the noise in the strips that contribute to that cluster. Each event is treated in the following way:

1. Look for hits above 5 σ, where σ is the noise of the strip after pedestal subtraction and common-mode noise correction.
2. Store the value of the highest hit divided by the noise of the corresponding channel for that time sample. This is referred to as signal/noise ratio and at the same time takes care of the normalization of the energy-loss distribution.
3. If one or both of the adjacent strips have a value above 1 σ, add the signal/noise ratio(s) to the cluster.
4. Histogram the signal/noise ratio of the cluster in the bin with the corresponding TDC value. Note that the content of the same channels is added for the other time samples, which gives seven additional entries each 25 ns apart in the 2 dimensional histogram.
5. Repeat steps 1-4 for the hits that have not yet been used in other clusters until all hits of this event are processed. If an event contains more than 4 clusters, it is considered noisy and discarded.

The result of this procedure is a plot like Fig. 8. Two slices of this plot, containing typical energy-loss distributions and fits, are shown in Fig. 11. The distribution in the peak of the pulse resembles a Landau and 25 ns later it is mostly Gaussian. The normalized χ^2-values are 1.1 for both fits, indicating that the convolution gives a good description of the data.

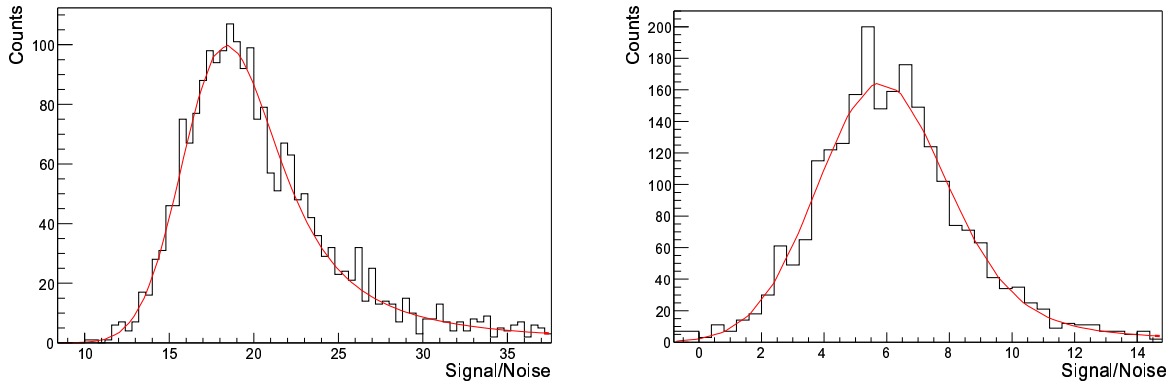

Figure 11: Energy-loss distributions for the cluster charge analysis of chip 8 with V_{fs} = 500 mV. Left the data from a 3 ns window around the peak and right from a 3 ns window 25 ns later (around the spill-over point).

The high statistics measurement for chips 8, 9, 10, 13, 14 and 15 (data set 2) enables the identification of trends within the chips. Sufficient data are available to determine the pulse shape characteristics for groups of twelve neighboring channels. The plots in Figs. 12 and 13 of peak amplitude, spill-over and peaking time differences[2] versus channel number, demonstrate clear trends as a function of channel number.

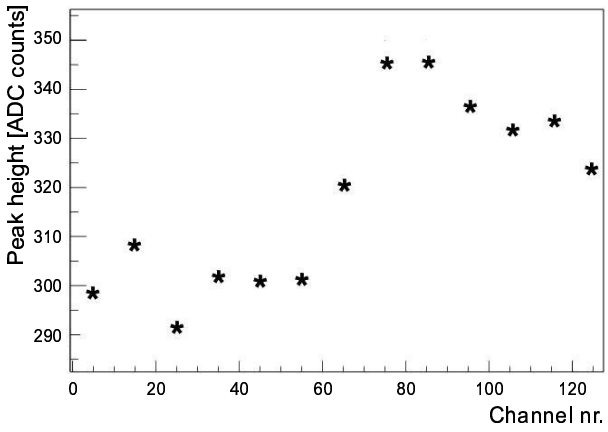

Figure 12: Peak amplitude versus channel number of chip 8.

The differences in pulse shape characteristics are visualized in Fig. 14 where the average pulse shape produced by channel numbers 5-45 is shown together with that produced by channel numbers 80-120.

The variations in the characteristics of the chip as function of channel number, as shown in Figure 12 and 13, hint to a problem in the chip. In fact, it relates to a problem that was first encountered in independent laboratory tests at both NIKHEF and Heidelberg: the first read-out after the one that contains a test pulse still contains a remainder of the test pulse, even when this read-out is delayed by 100 μs. This is explained by trapped charge in a capacitance of the read-out amplifier circuit of the Beetle chip that transfers ≈-35% of the signal to the next read-out. This phenomenon is baptized sticky charge [4]. The 8 consecutive samples used in the beam-test, together with the high statistics, make this problem also visible in the data. The resulting change of the pulse shape is illustrated schematically in Fig. 15. The analysis of the single time sample measurement in section 5.4 confirms a clear channel dependence and makes it possible to quantify the problem more accurately. Simulations indicate that this effect is time critical. It is caused by the simultaneous activation

[2]Peaking time is the time between the moments that the signal starts to rise and reaches its maximum. Only the difference in peaking time can accurately be determined because the start of the signal is difficult to detect.

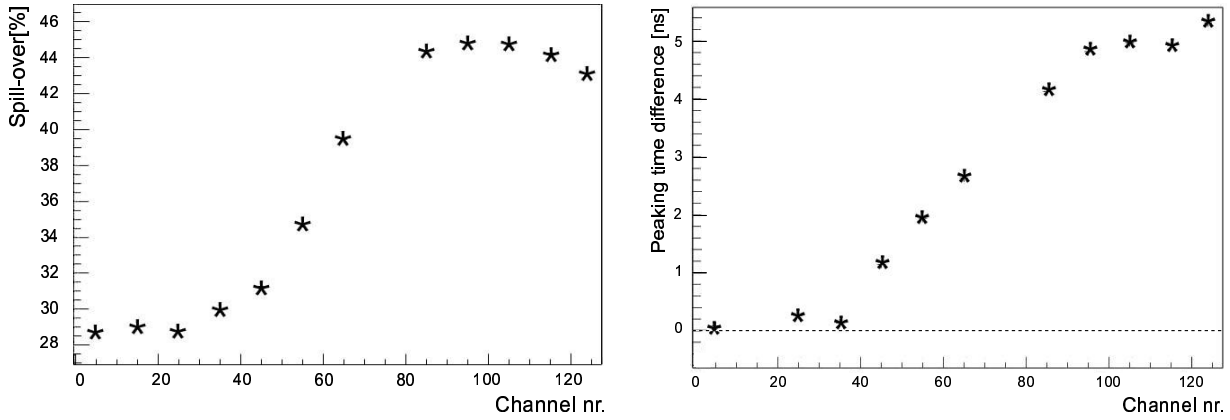

Figure 13: Spill-over (left) and peaking time differences (right) versus channel number of chip 8. The difference in peaking time is shown with respect to the first group of 12 channels.

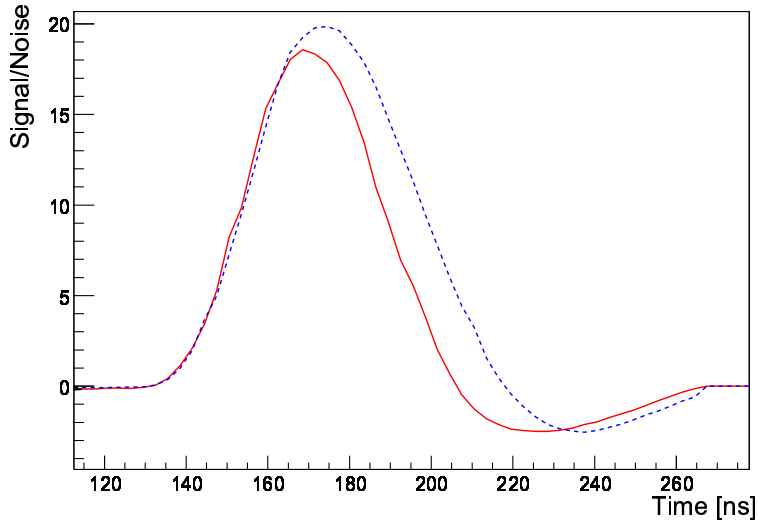

Figure 14: Pulse shapes for high (dashed line) and low (solid line) channel numbers of chip 8.

of two reset switches. The problem disappears if the activation of one of them is shifted by about 1 ns [20]. Due to small delays within the chip only the channels with low channel numbers are affected. In case of consecutive triggers, the sticky charge problem is effectively a tail cancellation, because these samples are only 25 ns apart. The problem is solved in the Beetle1.2 by a forced discharge of the capacitance of the read-out amplifier in between read-outs [10]. This is a patch that only works for non-consecutive read-outs. In the Beetle1.3 the sticky charge problem is solved completely [21] by changing the timing of the multiplexer circuit with respect to the read-out amplifier circuit by 5 ns, avoiding the simultaneous activation of the reset switches.

Channels with high channel numbers do not suffer from this sticky charge effect, which can be seen more clearly in section 5.4. Therefore, these channels can be used to make realistic predictions for the pulse shape of future chip versions. In the following analysis, all the numbers that are shown are based on the results of the channels with channel numbers 80-120. The channels 121-128 are excluded because the higher noise of these channels does not represent the average behavior of the chip (see Fig. 6).

The Beetles were programmed with various shaper settings to optimize the pulse shape for the VELO requirements. The dominant requirements are spill-over and signal/noise ratio. A setting was selected with 10-15% maximum undershoot. The shaper current was 32 μA and the pre-amplifier current was 350 μA. The feedback voltage of the shaper was varied to obtain 30% spill-over with the highest signal/noise ratio averaged over all channels. The results are presented in Table 4.

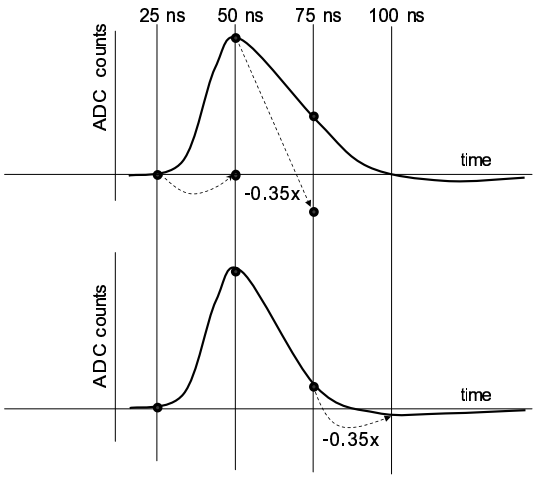

Figure 15: Sketch of the sticky charge effect: original pulse shape (top), affected pulse shape (bottom).

Chips 3, 4, 11 and 12 are connected to the regions with the longer strips. The input capacitance of these chips is larger and their performance is inferior to the performance of the other chips [9]. The difference between the two kinds of tails of the hybrid might affect the performance as well. The tail constructed with the solid copper layer is used for the chips with numbers 0 - 7 and the tail with the grid for chips 8 - 15. On average the performance of the high numbered chips is slightly better than that of the low numbered chips, which could indicate that the average parasitic capacitance is reduced when a grid is used.

In some cases chips 6, 7 and 15 have a lower signal/noise ratio because of increased system noise in the ADC. This is a problem related to ground loop currents and it spontaneously appeared and disappeared during the measurements. It was known that chip 7 and 15, which were connected to ADC input 7, suffer from this. But it became apparent that chip 6, which was connected to ADC input 5, had similar problems. Note the anomalous signal/noise ratios for chips 9 (low) and 10 (high) for the V_{fs} = 800 setting. This is not understood and should be verified in future beam-tests.

Table 4: Overview of the average pulse shape characteristics for channel numbers 80-120 (I_{sha} = 32 µA, I_{pre} = 350 µA).

	V_{fs} = 500 mV			V_{fs} = 700 mV			V_{fs} = 800 mV		
Chip nr.	S/N	RT [ns]	SO [%]	S/N	RT [ns]	SO [%]	S/N	RT [ns]	SO [%]
0	18.9±0.1	23.1±0.1	37.5±0.4	20.2±0.1	24.4±0.1	45.8±0.5	-	-	-
1	18.2±0.1	23.9±0.1	35.1±0.5	19.3±0.1	24.3±0.1	44.4±0.7	-	-	-
2	18.7±0.1	23.5±0.2	36.5±0.6	19.8±0.1	24.3±0.2	44.3±0.9	-	-	-
3	13.7±0.1	24.7±0.2	43.6±0.9	14.8±0.1	25.6±0.2	49.4±0.7	-	-	-
4	14.8±0.1	24.4±0.2	40.8±0.7	16.1±0.1	25.4±0.2	47.0±0.7	-	-	-
5	18.2±0.1	23.8±0.1	38.6±0.4	19.6±0.1	24.7±0.1	47.5±0.5	-	-	-
6*	16.2±0.1	24.4±0.2	35.9±0.6	16.7±0.1	24.3±0.2	43.5±0.7	-	-	-
7*	16.4±0.1	23.6±0.2	37.7±0.6	18.4±0.1	24.3±0.2	43.7±0.8	-	-	-
8	18.8±0.1	23.1±0.1	36.7±0.3	20.2±0.1	24.3±0.1	45.7±0.2	20.8±0.1	24.8±0.1	50.4±0.4
9	17.3±0.1	23.1±0.1	33.8±0.4	18.8±0.1	24.1±0.1	42.9±0.3	17.5±0.1	24.9±0.1	48.0±0.5
10	19.0±0.1	23.0±0.1	35.4±0.4	20.5±0.1	24.3±0.1	45.3±0.3	24.3±0.1	24.7±0.1	50.4±0.6
11	-	-	-	15.2±0.1	25.0±0.1	55.4±0.8	-	-	-
12	-	-	-	17.4±0.1	24.1±0.1	52.8±0.6	-	-	-
13	18.4±0.1	23.3±0.2	35.1±0.5	19.7±0.1	24.1±0.1	44.2±0.3	20.6±0.1	24.9±0.1	49.8±0.6
14	17.8±0.1	23.4±0.1	36.2±0.5	19.0±0.1	24.6±0.1	45.2±0.4	22.8±0.1	25.0±0.1	51.2±0.6
15*	17.2±0.1	23.4±0.2	34.6±0.6	18.6±0.1	23.9±0.1	44.0±0.4	22.7±0.1	24.3±0.1	48.0±0.6
*Higher system noise due to damaged DAQ channels									

The measured pulse shapes for the chips connected to the regions with the short strips (all but 3, 4, 11 and 12) are visualized in Fig. 16 and the simulated pulse shapes are shown in Fig. 17. The electrical circuits of the Beetle1.1 were designed with Cadence [22]. A SPICE netlist was extracted from the layout that included the parasitic capacitances in the front-end circuit. This information was used in HSpice, a numerical analysis package from METASOFT, to determine the expected time response. The accuracy of the time response of this kind of simulations is expected to be ≈10%.

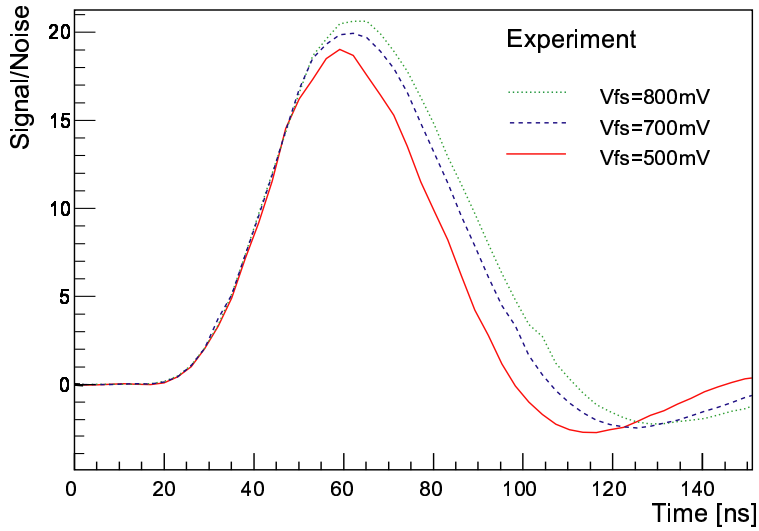

Figure 16: Overview of the MPVs of chip 8 for various bias settings. I_{sha} = 32 µA, I_{pre} = 350 µA, V_{fs} = 500 mV (solid line), 700 mV (dashed line) and 800 mV (dotted line). The lines connect the data points.

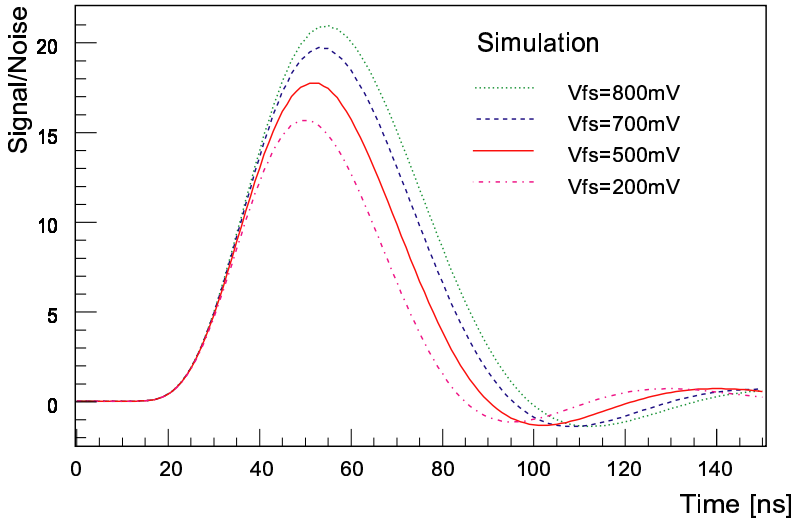

Figure 17: Overview of the pulse shape simulations for various bias settings. I_{sha} = 32 µA, I_{pre} = 350 µA, V_{fs} = 200 mV (dash-dotted line), 500 mV (solid line), 700 mV (dashed line) and 800 mV (dotted line).

The average results of the measurements for the chips connected to the regions with the short strips are summarized and compared to simulations in Table 5. The statistical error is the RMS value for the variations from chip to chip. The values for the signal/noise ratio found in the simulation are normalized to the measurements with V_{fs} = 800 mV. The signal/noise ratios for the other settings of the simulation are extrapolated based on the assumption that the noise does not change[3]. The simulations and measurements are in reasonable agreement. According to the simulations, faster pulses can be created by a further reduction of V_{fs} at the cost of a lower signal/noise ratio.

[3]This assumption is not completely correct: an increase of V_{fs} reduces the bandwidth of the shaper, which results in a reduction of the noise.

Table 5: Comparison of simulations with averages of the cluster charge analysis for various V_{fs} settings (I_{sha} = 32 µA, I_{pre} = 350 µA). The signal/noise ratio of the simulation is normalized at V_{fs} = 800 mV and extrapolated to the other settings based on the assumption that the noise is constant. The statistical error of the analysis is the RMS value for the variations from chip to chip.

	Signal/Noise		Rise time [ns]		Spill-over [%]	
	Simulated	Analyzed	Simulated	Analyzed	Simulated	Analyzed
V_{fs} = 500 mV	17.7	17.9±0.9	20.3	23.5±0.7	30	36.1±1.3
V_{fs} = 700 mV	19.7	19.2±1.0	20.7	24.3±0.2	35	44.7±1.3
V_{fs} = 800 mV	21.4	21.4±2.1	21.8	24.7±0.2	37	49.6±1.1

This section is concluded with a summary of the systematic errors of the cluster charge analysis. The contributions are added linearly. The effects are all discussed in section 4.2 except for a correction of the signal/noise ratio based on the results of the track selection analysis, which is discussed in section 5.3. The systematic error of the signal/noise ratio includes - 0.1 from the fit of the pulse shape, ± 0.1 from the bin size variations and - 0.7 from the track selection analysis. In total this adds up to an asymmetric error of (-0.9, +0.1). The systematic errors of the rise time and the spill-over consist only of contributions from bin size variations and are ± 0.5 ns and ± 1% (absolute value), respectively.

5.2 Strip charge analysis

The pulse shapes of signals from single strips are studied in what we will call the 'strip charge analysis'. For each event the strip with the highest signal/noise ratio is selected. For this strip the common-mode corrected signal/noise ratios of the 8 time samples are stored in a two dimensional histogram of amplitude versus time. The strip charge method is the simplest way to analyze the data. No knowledge is required about detector geometry, alignment, pitch adapter etc. A disadvantage of this method is that only a fraction of the charge is found if the charge is distributed over more than one strip. This results in broadening of the energy-loss distribution and a shift of the peak to a lower value. In this section the pulse shape characteristics are determined with the strip charge method and compared to the results of the cluster charge analysis. In Fig. 18 the signal distributions in a 3 ns window around the peak and 25 ns later (around the spill-over point) are presented for chip 8 with V_{fs} = 700 mV. The fits have χ^2-values of 1.1, which indicates that they give a good description of the data.

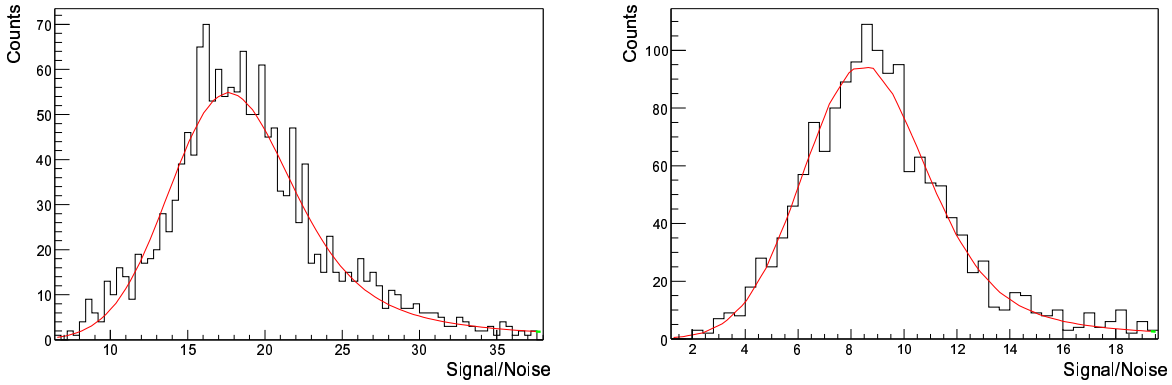

Figure 18: Energy-loss distributions and fits for the strip charge analysis of chip 8 with V_{fs} = 700 mV. Left the data from a 3 ns window around the peak and right from a 3 ns window 25 ns later (around the spill-over point).

In Table 6 the results of the strip charge analysis are compared to the cluster charge analysis for V_{fs} = 500 mV. The rise time and spill-over are almost identical but the signal/noise ratio in the peak of the pulse is 5 - 10% lower for the strip charge analysis. This is in accordance with the findings of [19] for a setup with signal/noise ratios comparable to ours. In the rest of this section we will show that lower signal/noise ratios found with this method are entirely due to the charge sharing between neighboring strips. This effect is described by the η-distribution, which represents the fraction of the cluster charge on the strip with the highest signal/noise ratio.

Table 6: Comparison of the strip charge and cluster charge analysis (I_{sha} = 32 µA, I_{pre} = 350 µA, V_{fs} = 500 mV).

	Strip charge analysis			Cluster charge analysis		
Chip nr.	Signal/Noise	Rise time [ns]	Spill-over [%]	Signal/Noise	Rise time [ns]	Spill-over [%]
0	17.9±0.1	24.6±0.1	35.6±0.5	18.9±0.1	23.1±0.1	37.5±0.4
1	16.9±0.1	23.5±0.1	37.2±0.5	18.2±0.1	23.9±0.1	35.1±0.5
2	17.3±0.1	23.8±0.2	35.6±0.7	18.7±0.1	23.5±0.2	36.5±0.6
3	11.8±0.1	24.6±0.2	44.2±0.8	13.7±0.1	24.7±0.2	43.6±0.9
4	13.3±0.1	24.5±0.2	40.6±0.7	14.8±0.1	24.4±0.2	40.8±0.7
5	17.4±0.1	24.1±0.1	38.2±0.4	18.2±0.1	23.8±0.1	38.6±0.4
6	15.3±0.1	23.9±0.1	37.5±0.5	16.2±0.1	24.4±0.2	35.9±0.6
7*	15.1±0.1	24.0±0.2	38.2±0.7	16.4±0.1	23.6±0.2	37.7±0.6
8	17.7±0.1	23.4±0.1	36.9±0.4	18.8±0.1	23.1±0.1	36.7±0.3
9	16.4±0.1	23.2±0.1	35.2±0.5	17.3±0.1	23.1±0.1	33.8±0.4
10	17.1±0.1	23.3±0.1	36.6±0.5	19.0±0.1	23.0±0.1	35.4±0.4
13	17.2±0.1	23.5±0.1	35.4±0.5	18.4±0.1	23.3±0.2	35.1±0.5
14	16.9±0.1	23.6±0.1	37.4±0.6	17.8±0.1	23.4±0.1	36.2±0.5
15*	15.5±0.1	23.5±0.2	35.8±0.7	17.2±0.1	23.4±0.2	34.6±0.6
*Higher system noise due to damaged DAQ channels No data available for chips 11 and 12						

In Fig. 19 the measured η-distribution is shown, in which the data with η > 0.9 are collected in the bin at η = 1 because in this region the charge on the second strip can not always be distinguished from the noise. In the same figure a parametrization of the η-distribution is shown normalized to the number of entries with η > 0.9, which matches the data reasonably well. The parametrization was calculated from a relation between η and the distance of the hit to the nearest strip, assuming that the incident particles are homogeneously distributed over the detector surface and that the charge is spread over at most 2 strips. This more intuitive relation is shown in Fig. 20. Due to geometrical arguments it is symmetric around the point where the distance is half the strip pitch, which lies in the middle between the two strips.

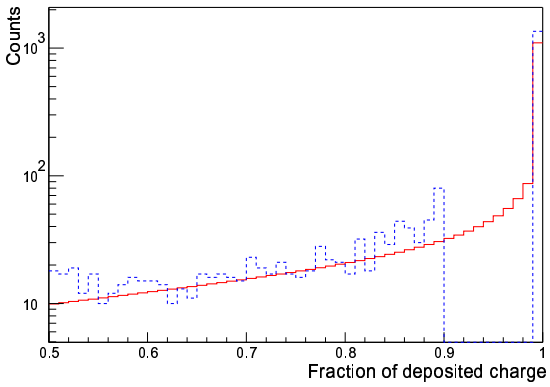

Figure 19: The η-distribution. The dashed histogram is calculated from the data and the solid one is a parametrization.

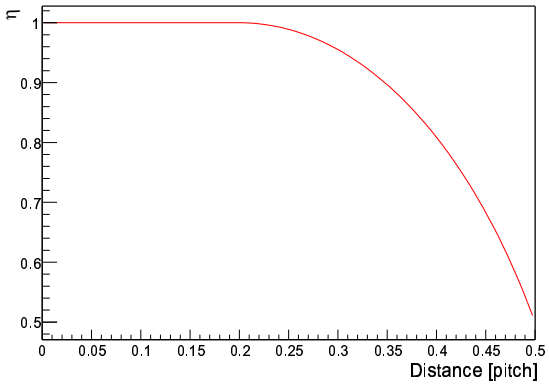

Figure 20: Relation between η and the distance of the hit to the nearest strip. The distance is expressed as fraction of the pitch.

Note that the width of the region with η = 1 in Fig. 20 matches half the strip width, which means that a hit directly on a strip is only supposed to deposit charge on that strip. A hit in the middle of two strips gives an η of 0.5. The distribution of the number of strips that contribute to a cluster is extracted from the data and shown in Fig. 21. In 92% of the cases the cluster size is one or two. For the other 8% a (most of the times small) error is introduced that corresponds to the charge that is not on the two strips nearest to the hit.

The parametrized η-distribution is used to calculate an expected result for the strip charge analysis. The entries in the histogram of the energy-loss distribution of the cluster charge analysis are redistributed with a folding procedure. A

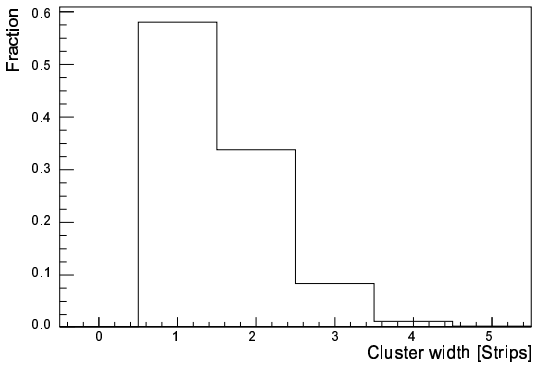

Figure 21: Number of strips that contribute to a cluster.

large fraction of the entries are folded with $\eta = 1$ and thus remain in the same bin. The remaining events move to lower signal/noise ratios according to the η-distribution. The result of this redistribution is compared to the histogram of the strip charge analysis in Fig. 22.

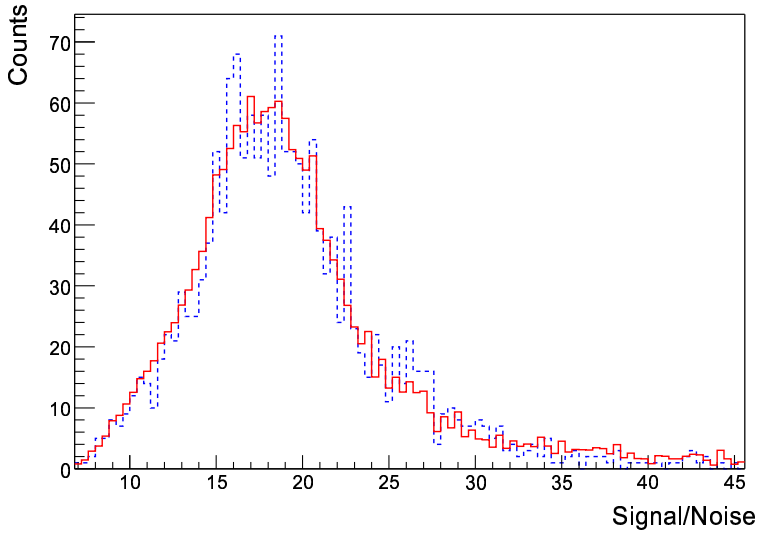

Figure 22: Comparison of the energy-loss distribution from the strip charge (dashed) analysis and the redistributed cluster charge (solid) using the η-distribution.

The two distributions agree very well. The distributions are fitted with a convolution of a Gauss and a Landau. All fit parameters match within 1.5 σ, where σ is the error of the parameter. The MPVs, which are the key parameters for the signal/noise ratios mentioned in Table 6, are equal within 0.5 σ. We conclude that the differences found between the results from the strip charge analysis and the cluster charge analysis can solely be attributed to charge sharing between strips.

5.3 Track selection analysis

In the 'track selection analysis' three strips nearest to the x and y coordinates found in an independent XY tracking station are selected[4]. For each of the eight time samples the signal/noise ratios of these strips are added and stored in a two dimensional histogram of amplitude versus time.

[4]The selection is based on the assumption that the tracks are perpendicular to the sensor plane. An independent measurement showed that the dispersion of the beam introduces an uncorrelated contribution to the resolution with a standard deviation of about 5 μm.

An advantage of the track selection method is that there is no a priori selection of strips based on signal/noise ratio, while the strip selection in the cluster charge method is entirely based on signal/noise ratio. A disadvantage of the 'track selection analysis' is that detailed knowledge is required of the detector bonding scheme, the detector strip geometry and the detector alignment with respect to the tracking station. A second disadvantage is that the amplitude is always the sum of the signal/noise ratios of three strips even if some of these strips carry no charge; these strips will only contribute to the width of the distribution. A third disadvantage is the dependence of the results on the quality of the track information. The strips that are selected may contain only a fraction of the charge or just noise because the track information is not sufficiently accurate. In Fig. 23 the distribution of the residuals between the predicted R coordinate of the tracking station and the cluster center in the Beetle detector is shown. The fitted Gaussian has a standard deviation of about 30 μm (varying slightly with run conditions). The data for the track selection analysis has been collected on the inner region of the Beetle detector, where the strip pitch is 32.5 μm.

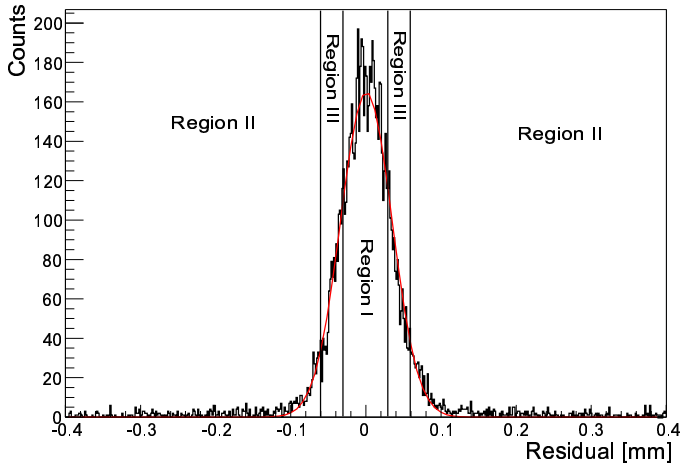

Figure 23: Residuals of the reconstructed tracks. The regions are used to compare the distance in units of strip pitch to the residuals.

In principal the resolution of the tracking station needs to be much smaller than the strip pitch to allow for accurate reconstruction of a cluster with the track selection method[5]. However, the data can still be used to determine the pulse shape characteristics and to compare them with the results of the cluster charge analysis. In Fig. 24 the energy-loss distributions in a 3 ns window around the peak and 25 ns later (around the spill-over point) are presented for chip 0 with V_{fs} = 500 mV. The first histogram shows a clearly separated peak around zero in addition to the expected Landau distribution, which is the result of insufficient track resolution. The peak is approximated with a Gaussian and subtracted from all slices to correct for this effect [6]. Note that in the second histogram of Fig. 24 the noise contribution can no longer be separated. The corrected distributions are shown in Fig. 25. In spite of the correction, the histogram of the 3 ns window around the spill-over point still has a much larger width than the histogram of Fig. 11, created with the cluster charge analysis. This might be explained by the selection of 3 strips, which should broaden the distribution[7].

The results of the track selection analysis are compared to the cluster charge analysis in Table 7 for V_{fs} = 500 mV. Only those results are given where sufficiently accurate track information and a sufficiently low noise background resulted in an acceptable normalized χ^2 for the fits to the energy-loss distributions. Chips 0, 5 and 13 give the most reliable results.

The track selection analysis results in almost identical values for the rise time and in significantly lower values for the signal/noise ratio and the spill-over. The systematic uncertainty in the spill-over is difficult to estimate, but the conservative approach is to assume that the lower spill-over is completely due to systematic effects caused by insufficient resolution in the track selection analysis.

In the rest of this section the observed differences in signal/noise ratio are discussed. An expected result for the track

[5]The best resolution obtained with this XY detector is 8 μm [23]. This resolution was only obtained under conditions with low noise levels. In our setup additional noise was introduced by the electronics that was used to match the DC-levels of the signals with that of the ADC.

[6]The Gaussian around zero has a slightly positive mean value and is broader than expected from the noise. This indicates that strips further away than two times the pitch can still receive some charge. This is also observed in Fig. 21. The width and the position of the Gaussian are scaled linearly with an estimation of the MPV to compensate for this effect.

[7]Hits that are almost 2 strips away give a small signal. In the tail of the pulse these hits can not be separated from the main Landau and broaden the shape as well.

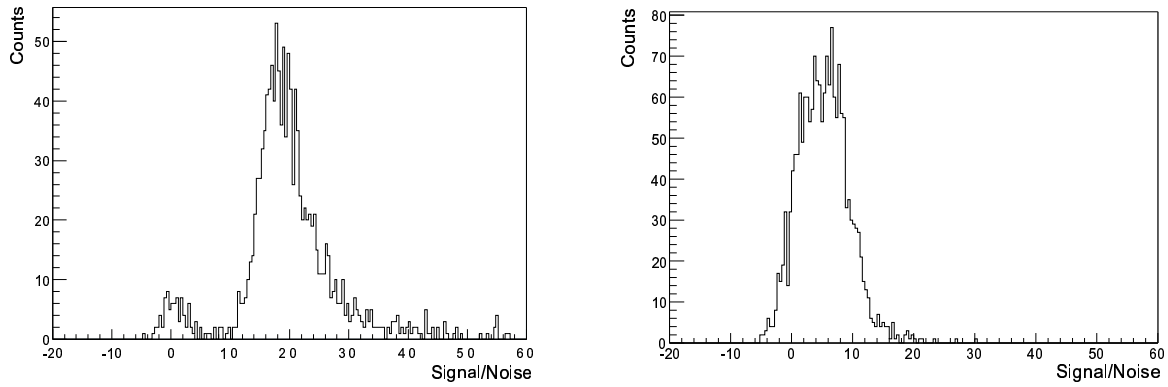

Figure 24: Energy-loss distributions for the track selection analysis of chip 0 with V_{fs} = 500 mV. Left the data from a 3 ns window around the peak and right from a 3 ns window 25 ns later (around the spill-over point).

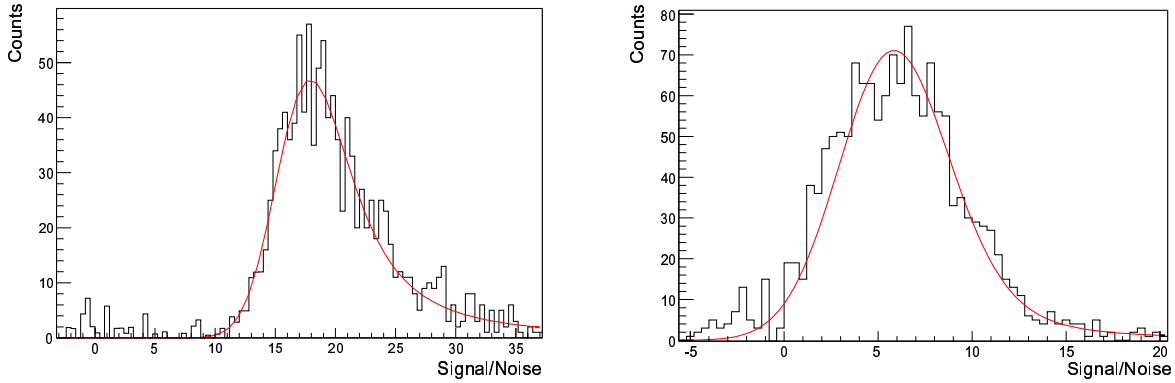

Figure 25: Corrected energy-loss distributions and fits for the track selection analysis of chip 0 with V_{fs} = 500 mV. Left the data from a 3 ns window around the peak and right from a 3 ns window 25 ns later (around the spill-over point).

selection method is determined from the energy-loss distribution obtained with the cluster charge analysis. Entries in the energy-loss histogram are redistributed in a way that depends on the measured residual distribution shown in Fig. 23. When the distance between the predicted R coordinate of the tracking station and the cluster center is less than one unit of strip pitch, the signal/noise ratio is not changed, because the signal/noise ratios of the 3 strips nearest to the predicted location are added together and will on average give the same signal/noise ratio as the cluster. Most of the hits will be in this range (region I in Fig. 23). When the residuals are larger than 2 units of strip pitch (regions II), the signal/noise ratios of the three strips will on average add up to zero. Thus a small fraction of the entries will be redistributed to a

Table 7: Comparison of the track selection and the cluster charge analysis (I_{sha} = 32 µA, I_{pre} = 350 µA, V_{fs} = 500 mV).

	Track selection analysis			Cluster charge analysis		
Chip nr.	Signal/Noise	Rise time [ns]	Spill-over [%]	Signal/Noise	Rise time [ns]	Spill-over [%]
0	18.3±0.1	23.1±0.1	32.5±0.6	18.9±0.1	23.1±0.1	37.5±0.4
1	18.5±0.1	23.7±0.3	Not available	18.2±0.1	23.9±0.1	35.1±0.5
2	18.0±0.1	23.7±0.3	26.6±0.9	18.7±0.1	23.5±0.2	36.5±0.6
5	17.5±0.1	23.8±0.2	32.0±0.7	18.2±0.1	23.8±0.1	38.6±0.4
6*	16.6±0.1	20.4±0.3	Not available	16.2±0.1	24.4±0.2	35.9±0.6
7*	16.9±0.1	22.7±0.2	26.3±0.9	16.4±0.1	23.6±0.2	37.7±0.6
13	17.6±0.1	22.8±0.2	29.9±0.8	18.4±0.1	23.3±0.2	35.1±0.5
*Higher system noise due to damaged DAQ channels The statistics or data quality of the chips that are not shown was insufficient for analysis						

Gaussian peak around zero with a standard deviation of $\sqrt{3}$. When the residuals are between 1 and 2 units of strip pitch (regions III in Fig. 23) only a fraction of the charge will be found on the three strips around the predicted position. The η-distribution is calculated by combining the relation between η and the distance to the nearest strip as shown in Fig. 20 with the resolution[8]. The entries in the energy-loss distribution are redistributed accordingly to lower signal/noise ratios.

In Fig. 26 the result of this redistribution of the energy-loss distribution obtained with the cluster charge analysis is compared to the result of the actual track selection analysis. A small shift can be observed between the distribution obtained in the track selection method and the expected distribution. The histograms are fitted with a convolution of a Landau and a Gauss. All the fit parameters match within 1.5 σ (where σ is the error of the parameter) except for the MPVs, which are the key parameters for the signal/noise ratios. For the track selection analysis the MPV is about 0.7 lower than for the cluster analysis, which matches the differences found in Table 7. Although the average signal/noise ratio is reduced by the redistribution, it does not significantly change the MPV. Hence, the small shift can not be explained by the finite resolution of the tracking station in combination with the η-distribution[9]. A possible bias in the cluster charge method is the choice of the cluster size, which is based on thresholds and selects only positive contributions to the signal/noise ratio. As the discrepancy can be an indication of a systematic effect of the cluster charge method, the observed difference is included in the systematic error.

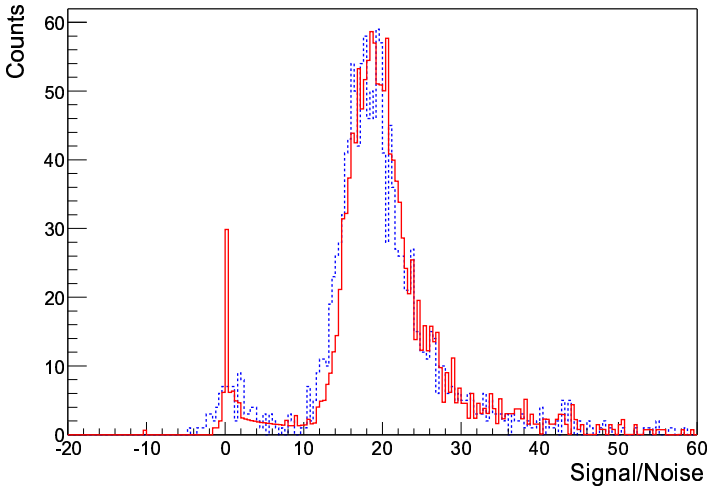

Figure 26: Comparison of the energy-loss distribution for the cluster charge and track selection analysis, using the η-distribution and the resolution. The solid histogram is created by redistributing the cluster charge and the dashed histogram with the track selection method.

5.4 Single time sample measurements

In the previous sections all data were acquired for 8 consecutive time samples. This allows the study of the complete pulse shape without shifting the latency. However, in the actual LHCb running conditions, data will only be collected in a single time sample. We also collected so-called single time sample data to investigate whether or not the performance of the Beetle depends on the number of consecutive samples. Independent runs were taken for 25 ns regions enclosing the peak, the rising edge and the tail of the pulse shape.

Single time sample data were taken for chips 0, 1, 2 , 5, 6 and 7 with V_{fs} = 700 mV. Track information is needed for the strip selection, in particular for an accurate reconstruction of the rising and falling edge of the pulse. Chip 0 is selected for this analysis because it has the highest statistics and the most accurate track reconstruction. The results are compared to the cluster charge analysis in Table 8. The systematic errors of the cluster charge analysis are included to allow for comparison between the two different analysis methods. The results are in good agreement, there is no degradation in performance if only one time sample of the Beetle is read-out.

Single time sample data are also used to get more accurate information about the sticky charge effect. The time difference between two successive triggers of the Beetle was about 10 ms. Therefore, the sticky charge effect cannot be

[8]The pitch on the x-axis of the η-distribution now ranges from 0 to 1 (instead of 0 to 0.5). Due to the convolution with this distribution a continuous background appears in the histogram between the noise around zero and the peak in the energy-loss spectrum around 20.

[9]The sensitivity of this result to the resolution and to the exact shape of the η-distribution is small. The MPV is dominated by the events with fully reconstructed charge, both in the tracking and in the cluster charge analysis.

Table 8: Comparison of the single time sample and the cluster charge analysis for chip 0 (I_{sha} = 32 µA, I_{pre} = 350 µA, V_{fs} = 700 mV). The systematic errors of the cluster charge analysis are included.

	Signal/Noise	Rise time [ns]	Spill-over [%]
Cluster charge analysis	$20.2\pm0.1\ ^{+0.1}_{-0.9}$	24.4±0.1±0.5	45.8±0.5±1
Single time sample analysis	19.6±0.1	25.0±0.3	45.6±0.5

caused by the pulse shaping circuitry of the front-end. This possibility could not be excluded from the data with multiple time samples. The magnitude of the sticky charge effect, as shown in Fig. 27, is the ratio of the signals in the current and preceding event. The horizontal bars in the figure correspond to the average values and the vertical bars indicate the standard deviations of the distributions. The figure shows that the sticky charge effect in the Beetle1.1 is large and negative for channel numbers below 40 and absent for channel numbers above 80. In the Beetle1.3 this problem is solved.

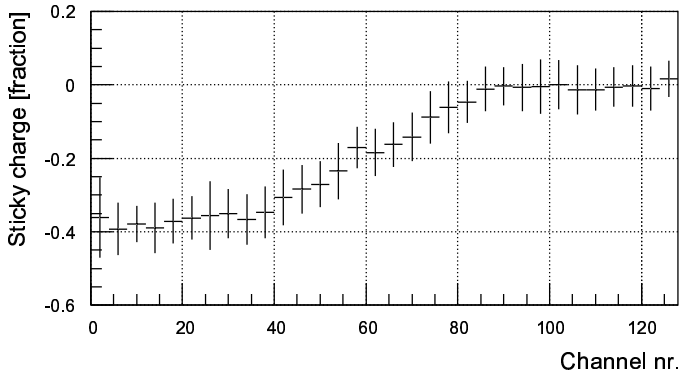

Figure 27: Sticky charge ratio as function of channel number.

5.5 High trigger rate analysis

The high trigger rate test was introduced to operate the chip under conditions where the read-out is almost continuously active. In that case, an incoming signal from the detector is processed during an ongoing read-out. Additional noise could be generated due to interference of the sampling and the read-out process. Test pulse triggers, each issuing the read-out of 4 consecutive time samples, were generated at a rate of 40 kHz. This occupied the Beetle read-out circuit for 64% of the time. These test pulse triggers were sent only to the Beetle, so the corresponding data were not acquired. In conjunction with the test pulse trigger, the physics trigger which is generated by the scintillators was passed both to the Beetle and the ADC, so these physics data were read-out and stored. The measurements were taken with V_{fs} = 700 mV.

Unfortunately a large fraction of the data is polluted with test pulses due to malfunctioning electronics. The data is filtered and collected in one histogram containing signal/noise ratios from the channels 80-120 of all available chips. The results are compared in Table 9 with the results from a combined data set of the cluster charge analysis. Except for the signal/noise ratio, the numbers are in good agreement. Although the average noise is slightly higher in case of the high trigger rate data, this does not account for the large difference between the two signal/noise ratios. So the decrease is caused by a lower signal in the data from the high trigger rate measurements compared to that of the other data. Maybe this can be attributed to interference of the test pulse circuit with the read-out, but the mechanism is yet unclear. More measurements are required to draw definite conclusions on this issue.

Table 9: Comparison of the high trigger rate and the cluster charge analysis (I_{sha} = 32 µA, I_{pre} = 350 µA, V_{fs} = 700 mV).

	Signal/Noise	Rise time [ns]	Spill-over [%]
Cluster charge analysis	19.2±0.1	24.3±0.1	44.7±0.1
High trigger rate	14.6±0.1	24.7±0.1	43.5±0.5

5.6 Efficiency, noise and spill-over

Although the pulse shape characteristics (signal/noise ratio, rise time and spill-over) are well suited to compare the performance of various settings and chips, they are not intuitively connected to the physics performance. A better approach is to show the efficiency of the Beetle detector versus the threshold in units of signal/noise ratio. This is done in Fig. 28 for region 0 of the sensor (see Fig. 2). The single time sample data with V_{fs} = 700 mV are used. The corresponding pulse shape characteristics are: signal/noise ratio = 19.6, rise time = 25.0 ns and spill-over = 45.6 %. The curve is generated by scanning the threshold from a signal/noise ratio of 5 to 45. The following steps are taken to create this figure.

1. Look for events with a hit in the selected region of the tracking station.
2. Try to match each hit found in the tracking station with a cluster above threshold in the Beetle detector within a window of 5 ns around the peak.
3. When all events are processed, the efficiency is equal to the number of clusters found in the Beetle detector divided by the number of selected events in the tracking station.

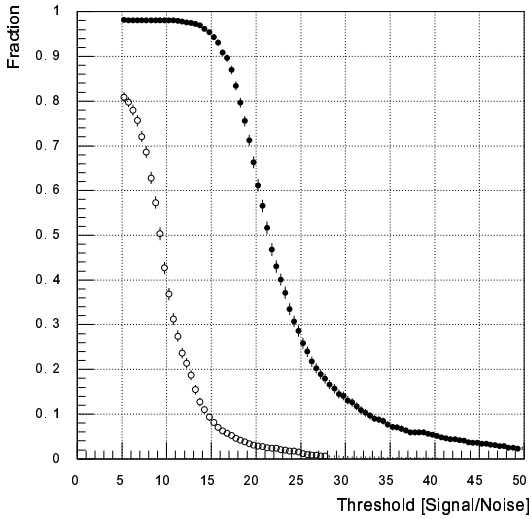

Figure 28: Efficiency (filled circles) and fraction of spill-over hits (open circles) as a function of threshold. The time window for accepted hits in the Beetle detector is 5 ns.

The curve starts at a threshold of 5 σ to avoid pollution of the plot with noise. For low thresholds almost all hits in the tracking station can be matched with a corresponding cluster in the Beetle detector. The few percent inefficiency is due to either a noise hit in the tracking station, a broken strip in the Beetle detector or a non-perpendicular track.

In the same plot the spill-over hits are drawn. This curve is generated the same way as the efficiency curve, however the sampling window for the Beetle detector is delayed by 25 ns. In the LHCb experiment the fraction of hits above threshold after 25 ns will pollute the physics data, since remnants of the hits will still be visible in the next bunch crossing.

The efficiency will almost be 100% when the threshold is set at a signal/noise ratio of 12, but about 20 to 25% of these hits will also be seen in the next bunch crossing. This can be reduced to 10% at the cost of about 3% efficiency-loss. Finding the optimal threshold setting for LHCb depends also on the tuning of the pulse shape and is beyond the scope of this document.

6 Conclusions

A prototype VELO hybrid was successfully designed, constructed and tested in a beam environment. The 16 Beetle1.1 chips were bonded without prior testing. They are all fully operational, which indicates a high yield of this deep submicron technology. The beam-test experiment showed no abnormal behavior of the chips due to their mounting closely together on a hybrid.

The majority of the data is analyzed with a method that uses cluster charges. This method is cross-checked both with a method that uses the signal/noise ratio of a single-strip and with a method based on track selection. The comparison

with the track selection analysis indicates a possible overestimation of about 0.7 in signal/noise ratio for the cluster charge analysis. This is included in the systematic error. Other small systematic uncertainties are due to the finite bin size and a slight tendency of the fit to overestimate the maximum value of the pulse. The pulse shape characteristics of the setting that complies best with LHCb specifications (I_{sha} = 32 μA, I_{pre} = 350 μA, V_{fs} = 500 mV) for the regions with the short strips are shown in Table 10 together with the results from simulation. If a slightly faster pulse is desired, the parameters can be re-tuned at the cost of a somewhat lower signal/noise ratio.

Table 10: Comparison of simulation with the average of the cluster charge analysis (I_{sha} = 32 μA, I_{pre} = 350 μA, V_{fs} = 500 mV). The statistical error of the analysis is the RMS value for the variations from chip to chip.

	Signal/Noise	Rise time [ns]	Spill-over [%]
analyzed	$17.9 \pm 0.9 \, ^{+0.1}_{-0.9}$	$23.5 \pm 0.7 \pm 0.5$	$36.1 \pm 1.3 \pm 1$
simulated	n.a.	20.3	30

Single time sample data and high trigger rate data are analyzed and found to be in good agreement with the rest of the results, except for the low signal/noise ratio of 14.6 of the high trigger rate analysis compared to 19.2 for the cluster charge analysis. This could be caused by interference from the test pulse circuit, but more measurements are required to draw definite conclusions on this issue. No other deteriorating effects are found due to these two specific aspects of LHCb operation. The single time sample data are also used to accurately determine the so-called sticky charge effect. This effect, where a fraction of the charge of a hit is carried over with a minus sign to the next read-out, is large for the channel numbers below 40 and is absent for channels with channel numbers above 80.

The analysis of efficiency and spill-over versus threshold shows that the Beetle can operate at about 97% efficiency with 10% spill-over hits. The Beetle pulse shape and the threshold settings need to be tuned together to get an optimal performance for LHCb.

Acknowledgments

We like to thank Joop Rövekamp for bonding the detector and the Beetle chips. We also like to thank the VELO group at CERN for their help with the preparation and running of the experiment and with the analysis.

References

[1] R. Brenner et al., RD-20 front-end architecture, Nucl. Instr. and Meth. A 339 (1994) 564.
[2] http://lhcb-tb.web.cern.ch/lhcb-tb/html/x7.htm
[3] Beetle reference manual, http://wwwasic.kip.uni-heidelberg.de/lhcb/Documentation.html
[4] N. van Bakel et al., Investigation of the Beetle1.1 chip in the X7 testbeam, LHCb 2002-053 revised version.
[5] http://www.eltech.com
[6] M. Feuerstack-Raible. Nucl. Instr. and Meth. A 447 (2000) 35.
[7] I2C-bus specification, http://www.semiconductors.philips.com/acrobat/literature/9398/39340011.pdf
[8] P. Gray and R.G. Meyer, Analysis and design of analog integrated circuits, ISBN 0-471-59984-0, 1993.
[9] Doris Eckstein, The LHCb Vertex Locator, LHCb 2003-099.
[10] Sven Löchner, http://wwwasic.kip.uni-heidelberg.de/lhcb/Meetings/Meeting220103/Beetle_Lab_Measurements.pdf
[11] M. Agari, Studies of the Beetle 1.2 Pipeline Homogeneity, LHCb 2003-155.
[12] H. Bichsel, Rev. Mod Phys 60 (1988) 663.
[13] S. Hancock et al., Phys. Rev. A 28 (1983) 615.
[14] http://wwwasdoc.web.cern.ch/wwwasdoc/shortwrupsdir/g110/top.html
[15] F.B. Hildebrand, Introduction to numerical analysis, ISBN 0-486-65363-3, 1956.
[16] V. Blobel, Formulae and methods in experimental data evaluation, Vol. 3, 1984.
[17] http://lhcbproject.web.cern.ch/lhcbproject/velo/testbeam/software/doc/veloroot/html/index.html
[18] http://root.cern.ch
[19] J. Libby, A simulation study of clustering in the VELO testbeam software, LHCb 2002-036.
[20] Daniel Baumeister, http://wwwasic.kip.uni-heidelberg.de/lhcb/Publications/LHCb_May2003_DB.pdf
[21] Sven Löchner, http://wwwasic.kip.uni-heidelberg.de/lhcb/Publications/LHCb_Nov2003.pdf
[22] Cadence DFII Software (version IC 4.4.3) with 0.25 μm (cmos6sf) CMOS Library Design Kit (version 1.0.2), 2001.
[23] E.N. Koffeman, Nucl. Instr. and Meth. A 452 (2000) 89.